Measurement of inclusive spin structure functions of the deuteron

J. Yun,[1] S. E. Kuhn,[1,*] G. E. Dodge,[1] T. A. Forest,[1,2] M. Taiuti,[3] G. S. Adams,[30] M. J. Amaryan,[39] E. Anciant,[5] M. Anghinolfi,[3] B. Asavapibhop,[24] G. Asryan,[39] G. Audit,[5] T. Auger,[5] H. Avakian,[18] S. Barrow,[15] M. Battaglieri,[3] K. Beard,[21] M. Bektasoglu,[1] W. Bertozzi,[23] N. Bianchi,[18] A. S. Biselli,[30] S. Boiarinov,[20] P. Bosted,[24] S. Bouchigny,[19] R. Bradford,[7] D. Branford,[13] W. K. Brooks,[35] S. Bueltmann,[37] V. D. Burkert,[35] C. Butuceanu,[10] J. R. Calarco,[26] D. S. Carman,[28] B. Carnahan,[8] C. Cetina,[16] L. Ciciani,[1] P. L. Cole,[34] A. Coleman,[10] J. Connelly,[16] D. Cords,[35,†] P. Corvisiero,[3] D. Crabb,[37] H. Crannell,[8] J. Cummings,[30] E. De Sanctis,[18] R. De Vita,[3] P. V. Degtyarenko,[35] R. A. Demirchyan,[39] H. Denizli,[29] L. C. Dennis,[15] K. V. Dharmawardane,[1] C. Djalali,[33] J. Domingo,[35] D. Doughty,[9,35] P. Dragovitsch,[15] M. Dugger,[4] S. Dytman,[29] M. Eckhause,[10] Y. V. Efremenko,[20] H. Egiyan,[10] K. S. Egiyan,[39] L. Elouadrhiri,[9,35] A. Empl,[30] L. Farhi,[5] R. Fatemi,[37] R. J. Feuerbach,[7] J. Ficenec,[38] K. Fissum,[23] A. Freyberger,[35] V. Frolov,[30] H. Funsten,[10] S. J. Gaff,[12] M. Gai,[11] G. Gavalian,[39] V. B. Gavrilov,[20] S. Gilad,[23] G. P. Gilfoyle,[32] K. L. Giovanetti,[21] P. Girard,[33] E. Golovatch,[25] C. I. O. Gordon,[17] K. A. Griffioen,[10] M. Guidal,[19] M. Guillo,[33] L. Guo,[35] V. Gyurjyan,[35] C. Hadjidakis,[19] D. Hancock,[10] J. Hardie,[9] D. Heddle,[9,35] P. Heimberg,[16] F. W. Hersman,[26] K. Hicks,[28] R. S. Hicks,[24] M. Holtrop,[26] J. Hu,[30] C. E. Hyde-Wright,[1] M. M. Ito,[35] D. Jenkins,[38] K. Joo,[37] C. Keith,[35] J. H. Kelley,[12] M. Khandaker,[27,35] K. Y. Kim,[29] K. Kim,[22] W. Kim,[22] A. Klein,[1] F. J. Klein,[35,8] A. V. Klimenko,[1] M. Klusman,[30] M. Kossov,[20] L. H. Kramer,[14,35] Y. Kuang,[10] J. Kuhn,[30] J. Lachniet,[7] J. M. Laget,[5] D. Lawrence,[24] G. A. Leksin,[20] K. Loukachine,[38,8] R. W. Major,[32] J. J. Manak,[35] C. Marchand,[5] S. McAleer,[15] J. W. C. McNabb,[7] J. McCarthy,[37] B. A. Mecking,[35] M. D. Mestayer,[35] C. A. Meyer,[7] R. Minehart,[37] M. Mirazita,[18] R. Miskimen,[24] V. Mokeev,[25] S. Morrow,[19] V. Muccifora,[18] J. Mueller,[29] L. Y. Murphy,[16] G. S. Mutchler,[31] J. Napolitano,[30] S. O. Nelson,[12] S. Niccolai,[16] G. Niculescu,[28] B. Niczyporuk,[35] R. A. Niyazov,[1] M. Nozar,[35] G. V. O'Rielly,[16] M. S. Ohandjanyan,[39] A. Opper,[28] M. Ossipenko,[25] K. Park,[22] Y. Patois,[33] G. A. Peterson,[24] S. Philips,[16] N. Pivnyuk,[20] D. Pocanic,[37] O. Pogorelko,[20] E. Polli,[18] B. M. Preedom,[33] J. W. Price,[6] D. Protopopescu,[17] L. M. Qin,[1] B. A. Raue,[14,35] G. Riccardi,[15] G. Ricco,[3] M. Ripani,[3] B. G. Ritchie,[4] S. Rock,[24] F. Ronchetti,[18] P. Rossi,[18] D. Rowntree,[23] P. D. Rubin,[32] K. Sabourov,[12] C. W. Salgado,[27] V. Sapunenko,[3] M. Sargsyan,[39] R. A. Schumacher,[7] V. S. Serov,[20] Y. G. Sharabian,[39] J. Shaw,[24] S. M. Shuvalov,[20] S. Simionatto,[16] A. Skabelin,[23] E. S. Smith,[35] L. C. Smith,[37] T. Smith,[26] D. I. Sober,[8] L. Sorrell,[24] M. Spraker,[12] S. Stepanyan,[39,1] P. Stoler,[30] S. Taylor,[31] D. Tedeschi,[33] U. Thoma,[35] R. Thompson,[29] L. Todor,[7] T. Y. Tung,[10] C. Tur,[33] M. F. Vineyard,[36] A. Vlassov,[20] K. Wang,[37] L. B. Weinstein,[1] H. Weller,[12] R. Welsh,[10] D. P. Weygand,[35] S. Whisnant,[33] M. Witkowski,[30] E. Wolin,[35] M. H. Wood,[35] A. Yegneswaran,[35] B. Zhang,[23] J. Zhao,[23] and Z. Zhou[23]

(CLAS Collaboration)

[1]*Old Dominion University, Department of Physics, Norfolk, Virginia 23529*

[2]*Center for Applied Physics Studies, Louisiana Tech University, Ruston, Louisiana 71272*

[3]*Istituto Nazionale di Fisica Nucleare, Sezione di Genova e Dipartimento di Fisica dell'Università, 16146 Genova, Italy*

[4]*Arizona State University, Department of Physics and Astronomy, Tempe, Arizona 85287*

[5]*CEA Saclay, DAPNIA-SPhN, F91191 Gif-sur-Yvette Cedex, France*

[6]*University of California at Los Angeles, Department of Physics and Astronomy, Los Angeles, California 90095-1547*

[7]*Carnegie Mellon University, Department of Physics, Pittsburgh, Pennsylvania 15213*

[8]*Catholic University of America, Department of Physics, Washington, D.C. 20064*

[9]*Christopher Newport University, Newport News, Virginia 23606*

[10]*College of William and Mary, Department of Physics, Williamsburg, Virginia 23187*

[11]*University of Connecticut, Physics Department, Storrs, Connecticut 06269*

[12]*Duke University, Physics Building TUNL, Durham, North Carolina 27706*

[13]*Department of Physics and Astronomy, Edinburgh University, Edinburgh EH9 3JZ, United Kingdom*

[14]*Florida International University, Miami, Florida 33199*

[15]*Florida State University, Department of Physics, Tallahassee, Florida 32306*

[16]*George Washington University, Department of Physics, Washington, D.C. 20052*

[17]*University of Glasgow, Glasgow G12 8QQ, United Kingdom*

[18]*Istituto Nazionale di Fisica Nucleare, Laboratori Nazionali di Frascati, P.O. 13, 00044 Frascati, Italy*

[19]*Institut de Physique Nucleaire d'Orsay, IN2P3, Boîte Postale 1, 91406 Orsay, France*

[20]*Institute of Theoretical and Experimental Physics, 25 B. Cheremushkinskaya Street, Moscow, 117259, Russia*

[21]*James Madison University, Department of Physics, Harrisonburg, Virginia 22807*

[22]*Kyungpook National University, Department of Physics, Taegu 702-701, South Korea*

[23]*Massachusetts Institute of Technology, Cambridge, Massachusetts 02139-4307*

[24]*University of Massachusetts, Department of Physics, Amherst, Massachusetts 01003*

[25]*University of Moscow, Moscow 119899, Russia*

[26]*University of New Hampshire, Department of Physics, Durham, New Hampshire 03824*

[27]*Norfolk State University, Norfolk, Viginia 23504*

[28]*Ohio University, Department of Physics, Athens, Ohio 45701*

[29]*University of Pittsburgh, Department of Physics and Astronomy, Pittsburgh, Pennsylvania 15260*
[30]*Rensselaer Polytechnic Institute, Department of Physics, Troy, New York 12181*
[31]*Rice University, Bonner Lab, Box 1892, Houston, Texas 77251*
[32]*University of Richmond, Department of Physics, Richmond, Virginia 23173*
[33]*University of South Carolina, Department of Physics, Columbia, South Carolina 29208*
[34]*University of Texas at El Paso, Department of Physics, El Paso, Texas 79968*
[35]*Thomas Jefferson National Accelerator Facility, 12000 Jefferson Avenue, Newport News, Virginia 23606*
[36]*Union College, Department of Physics, Schenectady, New York 12308*
[37]*University of Virginia, Department of Physics, Charlottesville, Virginia 22903*
[38]*Virginia Polytechnic and State University, Department of Physics, Blacksburg, Virginia 24061*
[39]*Yerevan Physics Institute, 375036 Yerevan, Armenia Pittsburgh, Pennsylvania 15213*
(Received 18 December 2002; published 19 May 2003)

We report the results of a new measurement of spin structure functions of the deuteron in the region of moderate momentum transfer [$Q^2=0.27$–1.3 $(\mathrm{GeV}/c)^2$] and final hadronic state mass in the nucleon resonance region ($W=1.08$–2.0 GeV). We scattered a 2.5 GeV polarized continuous electron beam at Jefferson Lab off a dynamically polarized cryogenic solid state target ($^{15}ND_3$) and detected the scattered electrons with the CEBAF large acceptance spectrometer. From our data, we extract the longitudinal double spin asymmetry $A_{||}$ and the spin structure function g_1^d. Our data are generally in reasonable agreement with existing data from SLAC where they overlap, and they represent a substantial improvement in statistical precision. We compare our results with expectations for resonance asymmetries and extrapolated deep inelastic scaling results. Finally, we evaluate the first moment of the structure function g_1^d and study its approach to both the deep inelastic limit at large Q^2 and to the Gerasimov-Drell-Hearn sum rule at the real photon limit ($Q^2\rightarrow 0$). We find that the first moment varies rapidly in the Q^2 range of our experiment and crosses zero at Q^2 between 0.5 and 0.8 $(\mathrm{GeV}/c)^2$, indicating the importance of the Δ resonance at these momentum transfers.

DOI: 10.1103/PhysRevC.67.0452XX PACS number(s): 13.60.Hb, 13.88.+e, 14.20.Dh

I. INTRODUCTION

The nucleon spin structure functions $g_1^{p,n}(x)$ and $g_2^{p,n}(x)$ and their moments have been extensively studied over the past two decades [1–10]. At large momentum transfer [$Q^2 \gg 1$ $(\mathrm{GeV}/c)^2$] and final state mass ($W>2$ GeV) these data can be successfully described via perturbative QCD (pQCD) up to next-to-leading order (NLO) and give us access to the helicity-weighted distribution functions $\Delta q(x)$ and $\Delta G(x)$ of quarks and gluons in the nucleon [11–14]. In this kinematic regime, one can relate the first moments $\Gamma_1^N = \int_0^1 g_1^N(x)dx$ of the spin structure functions $g_1^N(x)$ ($N=p$ or n) to the fraction of the nucleon spin carried by the quark helicities and, via the famous Bjorken sum rule [15,16], to the weak axial form factor g_A.

At lower momentum transfers, $Q^2 \approx 1$ $(\mathrm{GeV}/c)^2$, corrections proportional to powers of $1/Q^2$ develop due to higher twist and target mass effects [17–19] in addition to the logarithmic Q^2 dependence predicted by pQCD. As Q^2 decreases, an increasing part of the kinematic range $x=0$–1 lies in the region of resonant final states ($W<2$ GeV), which begin to dominate the spin structure functions. They become less positive (or more negative in the case of the neutron), in particular in the region of the Δ resonance. Data in this region on structure functions and on the (virtual) photon asymmetries A_1 and A_2 for the proton and the neutron,

$$A_1=\frac{\sigma_{1/2}-\sigma_{3/2}}{\sigma_{1/2}+\sigma_{3/2}}=\frac{g_1-g_2/\tau}{F_1},$$

$$A_2=\frac{\sigma_{LT}}{\sigma_{1/2}+\sigma_{3/2}}=\frac{g_1+g_2}{\sqrt{\tau}F_1}, \tag{1}$$

can help us unravel the spin-isospin structure of resonance transition amplitudes and their interference with each other and with nonresonant terms. We can also test whether the observed duality between unpolarized deep inelastic and resonant structure functions [20–22] is realized for spin structure functions as well [23,24]. Here, $\sigma_{1/2}$ and $\sigma_{3/2}$ are the (virtual) photon absorption cross sections for total (photon plus nucleon) helicity $\frac{1}{2}$ and $\frac{3}{2}$ and σ_{LT} is the longitudinal-transverse interference cross section, F_1 is the unpolarized structure function, and $\tau=\nu^2/Q^2$ with $\nu=E-E'$ being the energy loss of the scattered electron.

Due to the dominance of the resonances at low Q^2, the integrals Γ^p and $\Gamma^d \approx (\Gamma^p+\Gamma^n)/2$ (which are positive in the scaling region of high Q^2) decrease rapidly and become negative as Q^2 approaches zero. In the limit $Q^2\rightarrow 0$, the first moments for the proton and the neutron are constrained by the Gerasimov-Drell-Hearn (GDH) sum rule [25,26], which predicts that

$$\Gamma_1^N(Q^2)\rightarrow \frac{Q^2}{16\pi^2\alpha}\int_{\nu_{thr}}^{\infty}(\sigma_{1/2}-\sigma_{3/2})\frac{d\nu}{\nu}=-\frac{Q^2}{8M^2}\kappa_N^2. \tag{2}$$

*Corresponding author. Email address: skuhn@odu.edu
†Deceased.

Here, α is the fine structure constant and M and κ_N are the mass and anomalous magnetic moment of the nucleon, respectively. Since the GDH sum rule is negative, the integrals $\Gamma_1^{p,d}(Q^2)$ must have a negative slope at $Q^2=0$ and then change rapidly at low Q^2 to meet the positive experimental results in the deep inelastic scattering (DIS) region.

So far, only phenomenological models for $\Gamma_1(Q^2)$ covering the whole range of Q^2 exist [27–33]. These models are constrained to reach the large-Q^2 asymptotic value of the integral as measured by deep inelastic data and to approach zero at the photon point with a slope given by the Gerasimov-Drell-Hearn sum rule, Eq. (2). The authors of Refs. [28,29] use a simple parametrization of the integral $\Gamma_{1+2}=\int[g_1(x)+g_2(x)]dx$ to interpolate between these two points, and then subtract the integral over g_2 which is given by the Burkardt-Cottingham sum rule [34]. The approach taken in Refs. [30–32] uses a parametrization of existing resonance data and a vector meson dominance inspired interpolation of the remaining integral strength at the two end points.

For a complete picture of spin structure functions and their moments, one needs information on both the proton and the neutron. Since free neutron targets are impractical, deuterium (as in the experiment described here) or ^{3}He targets are used instead. An unambiguous extraction of neutron spin structure functions from nuclear ones is less straightforward in the resonance region than in the deep inelastic regime; however, the integrals Γ_1^N are much less affected by uncertainties from Fermi motion, off-shell effects, and other nuclear corrections [35–37]. In particular, studies [38,39] show that the integral Γ_1^d for the deuteron from pion threshold on up is very close to the incoherent sum of the proton and neutron integrals, once a correction for the deuteron D state has been applied.

So far, only very limited spin structure function data exist in the region of low to moderate Q^2 and W [40,41], especially on the deuteron. A large program is underway at Jefferson Lab to map out the entire kinematic region $Q^2 \approx 0.05$–$5\ (\mathrm{GeV}/c)^2$ and $W \leqslant 3$ GeV. This program consists of measurements on ^{3}He (in hall A) and on proton and deuteron targets with the CEBAF large acceptance spectrometer (CLAS) (the EG1 collaboration in hall B). First results from CLAS [42] and hall A [43] have already been published.

In the present paper, we present results on the deuteron from the first EG1 run in 1998, in which we measured double spin asymmetries $A_{||}=D(A_1+\eta A_2)$ on deuterium with a beam energy of 2.5 GeV. (D and η are kinematical factors, see Sec. IV.) These data cover a range in Q^2 from 0.27–$1.3\ (\mathrm{GeV}/c)^2$ and final state mass in the resonance region ($W=1.08$–2.0 GeV). The remaining dataset from EG1 is presently under analysis and will increase both the kinematic coverage and the statistical precision of our data significantly.

In the following, we give some details on the experiment (Sec. II) and its analysis (Sec. III). We present our results on the deuteron spin asymmetry $(A_1^d+\eta A_2^d)(W,Q^2)$, the structure function $g_1^d(x,Q^2)$ and its first moment $\Gamma_1^d(Q^2)$ (Sec. IV), and conclude with a summary and outlook (Sec. V).

II. EXPERIMENTAL DETAILS

The data described in this paper were collected during a three-month run in 1998, as part of the EG1 run group in Jefferson Lab's hall B. A polarized electron beam with 2.5-GeV beam energy was scattered off a deuterated ammonia ($^{15}ND_3$) target that was dynamically polarized along the beam direction. The average beam current of 2.5 nA corresponded to an instantaneous luminosity of $0.4 \times 10^{34}\ \mathrm{cm}^{-2}\,\mathrm{s}^{-1}$. The beam polarization was measured periodically with a Møller polarimeter and the average beam polarization was 72%.

We used the CLAS to detect the scattered electrons. The CLAS detector [44] is built around six superconducting coils that produce a toroidal magnetic field. The orientation of the magnetic field can be chosen so that electrons are bent either toward (inbending) or away from the beam line (outbending). The target was placed 55 cm upstream from its normal location in the center of CLAS to lower the angular threshold for electron detection and thus decrease the lower limit on the momentum transfer. Inbending electrons were detected down to a minimum polar angle of 14°. During this experiment the geometry of the target excluded particle tracks with a polar angle between 50° and 75°. The ϕ acceptance is $\approx 85\%$, limited mainly by the torus coils.

The CLAS detector package consists of three layers of drift chambers for track reconstruction, one layer of scintillators for time-of-flight measurements, forward Cherenkov counters for electron-pion discrimination, and electromagnetic calorimeters to identify electrons and neutral particles. A coincidence between the Cherenkov and the calorimeter triggers the data acquisition. Electron particle identification is accomplished using the Cherenkov detector and the distribution of energy deposited in the calorimeter. The large acceptance of CLAS (≈ 1.5 sr for electrons) and its large kinematic coverage offset the limited luminosity that can typically be reached with polarized solid state targets (of order $10^{35}\ \mathrm{cm}^{-2}\,\mathrm{s}^{-1}$ at best), and allowed us to collect data for the entire W and Q^2 ranges simultaneously.

The longitudinally polarized target was designed to fit within the 1-m central bore of the CLAS [45]. A pair of superconducting Helmholtz coils provided a 5-T magnetic field along the direction of the electron beam. The magnetic field was uniform to better than 1×10^{-4} in the center of the target over a length of 2 cm and a diameter of 2 cm. The ammonia crystals were contained within a plastic cylindrical cell 1 cm in length and 1.5 cm in diameter. The cell was immersed in a liquid He bath maintained at approximately 1 K by a ^{4}He evaporation refrigerator. The cell was mounted on a target insert that also held a NH_3 cell, as well as a ^{12}C and an empty cell. The latter cells were used to study the dilution of the measured asymmetries by events from unpolarized target constituents (see Sec. III C). The deuterons in the target were polarized using the dynamic nuclear polarization (DNP) technique [46,47] with 140 GHz microwaves. The polarization of the target was monitored online using the NMR technique. The NMR results were not used for our final analysis; instead, we extracted the product of beam and target polarization directly from our data, as described in

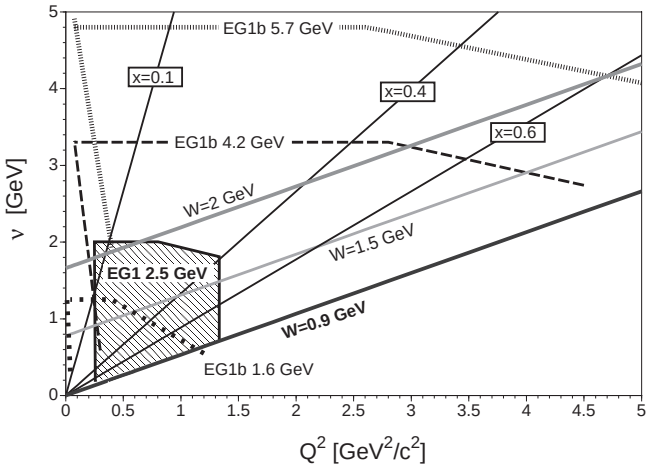

FIG. 1. Kinematic coverage of the data described in this paper (EG1 2.5 GeV) together with the kinematic range of the second run of EG1 (EG1b at 1.6 GeV, 4.2 GeV, and 5.7 GeV). The heavy solid lines indicate the elastic peak ($W=0.9$ GeV), the location of the S_{11} resonance ($W=1.5$ GeV) and the deep inelastic limit ($W=2$ GeV). Also shown are the kinematic lines for three representative values of x.

Sec. III C. The beam was rastered on the ND_3 target, although not over the full face of the target. The deuteron polarization suffered from this incomplete raster and from inadequate microwave power and ranged from approximately 10% to 25%. All data were taken with the target polarization along the beam direction, without reversal of the target polarization. The beam helicity was reversed every second.

During the 1998 run, we collected 300×10^6 triggers for an integrated beam charge of about 0.4 mC. From this sample, 100×10^6 electron events passed the cuts described in Sec. III A. These events covered a kinematic region from the quasielastic region ($W\approx0.94$ GeV) to the edge of the deep inelastic region ($W=2$ GeV) and for $Q^2=0.27-1.3$ $(\mathrm{GeV}/c)^2$. This kinematic coverage is shown in Fig. 1, together with the coverage of the second part of the EG1 experiment.

III. DATA ANALYSIS

The goal of our analysis was to first determine the double spin asymmetry

$$A_{||}=\frac{\sigma^{\uparrow\downarrow}-\sigma^{\uparrow\uparrow}}{\sigma^{\uparrow\downarrow}+\sigma^{\uparrow\uparrow}} \tag{3}$$

for each kinematic bin and then to extract the physical quantities of interest, the virtual photon asymmetries $A_1^d+\eta A_2^d$ and the structure function g_1^d, from the results. Here, $\sigma^{\uparrow\downarrow}$ stands for the differential electron scattering cross section with the target and electron spin pointing in opposite directions along the beam and correspondingly $\sigma^{\uparrow\uparrow}$ for parallel target and electron spin.

A. Data selection

For the present analysis, we selected data runs taken with a torus current of $+2250$ A (inbending electrons) and target polarization parallel to the beam direction. The data were taken with two slightly different beam energies, 2.494 GeV and 2.565 GeV, due to a change of the accelerator configuration. We separated our sample into four different ''run groups,'' two each with beam energy 2.494 GeV and 2.565 GeV. Each run group corresponds to a contiguous set of runs with the same target material and approximately constant target parameters and running conditions. Only runs with stable beam and detector performance were included in our sample. The 2.565 GeV groups also contained carbon target runs that were used to determine the dilution factor (see Sec. III C). We analyzed events with scattering angles from about 14° to 50° and scattered electron energies from 0.5 GeV to 2.5 GeV.

The data were sorted according to the helicity of the electron beam. During our run, the beam helicity followed a ''pseudorandom'' pattern of helicity pairs, where the first ''bucket'' (of 1 sec length) of each pair was given random helicity and the second its complement. We matched the sequence of helicity bits for each event with the pattern sequence recorded in helicity scalers and discarded pairs for which the helicity assignment was inconsistent. We also discarded pairs with significantly different (by more than 10%) beam intensities in the two buckets (due to beam fluctuations or trips). The final data sample contained only matched pairs of buckets with stable running conditions.

All events were accumulated in small bins of W ($\Delta W=0.02$ GeV) and Q^2 ($\Delta Q^2/Q^2\approx20\%$), separately for both beam helicities. (The data on asymmetries and g_1, shown in Sec. IV, are weighted averages of several such bins.) In addition, we also accumulated the integrated beam charge for each of the helicity buckets (corrected for deadtime) to normalize the helicity-sorted counts in each bin. We found that on average there was a 0.3% difference between the integrated charge for the two opposite helicities, possibly stemming from the sensitivity of the photocathode in the polarized source to small remaining linear polarization components or beam motions of the photoionization laser beam. Our normalization method removed the effect of this asymmetry, and it was further suppressed by reversing the relative sign between the helicity at the cathode and in the experimental Hall (through spin precession in the injector and the accelerator).

B. Electron cuts

We selected electron events by first requiring a negative track with matching signals in the time-of-flight (ToF) scintillators, the Cherenkov counters (CC), and the electromagnetic calorimeter (EC). In the presence of several such tracks, the track with the shortest flight time was selected as the electron candidate. Some additional cuts on the track vertex along the beam line removed events from the entrance and exit windows of the polarized target chamber, as well as badly reconstructed tracks.

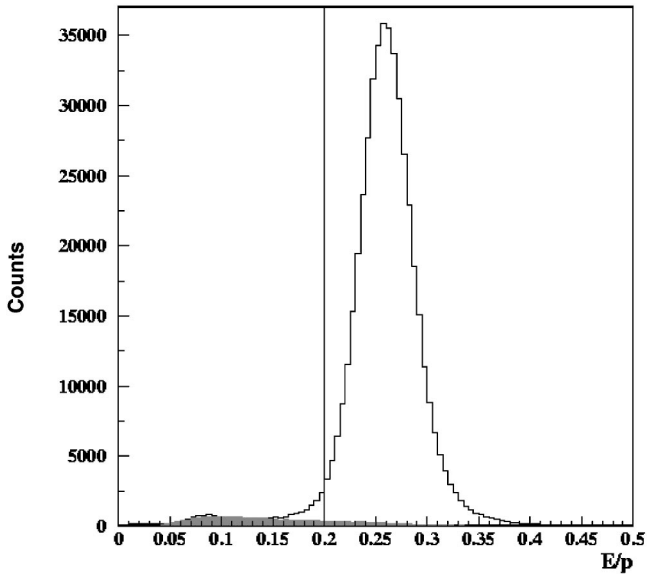

FIG. 2. Spectra of the ratio of measured energy E (in GeV) in the electromagnetic calorimeter over the track momentum, p (in GeV/c), for electrons (open histogram) and pions (shaded area). The vertical scale is arbitrary. Both spectra have been cross normalized at low E/p. Events above the indicated threshold are identified as electrons.

We used information from the CC and the EC to further separate electrons from negative pions. We required a signal in the CC that exceeded 50% of the average signal for a single photoelectron. Furthermore, we required that the energy measured in the EC exceeded 20% of the candidate electron momentum (the average sampling fraction of the EC was 27%). A typical example for the ratio of sampled EC energy over momentum is shown in Fig. 2. The open histogram shows events that passed all other electron cuts (including the CC cut).

We also collected a sample of π^- events with no signal above threshold in the CC. As shown by the shaded area in Fig. 2, the E/p spectrum associated with π^- events is strikingly different from the electron spectrum. Under the conservative assumption that *all* events below an E/p ratio of 0.15 came from pions, we cross normalized the two spectra below that point and estimated the remaining pion contamination of our electron sample by the ratio of the two integrated spectra above our cut of $E/p>0.2$. For all kinematics studied, this remaining contamination turned out to be less than 1%.

The reconstructed momenta of the scattered electrons were corrected for effects from unknown torus field distortions and slight drift chamber misalignments. We used NH_3 runs taken interleaved with the ND_3 ones to determine the correction factor by optimizing the position and width of the elastic peak ($W=0.938$ GeV) for all scattering angles θ and ϕ. The resulting corrections were of the order 0.1% on average.

C. Dilution and polarization

The double spin asymmetry $A_{||}$ can be extracted from the count rate asymmetry (normalized by the integrated beam charge) after accounting for the dilution from unpolarized target constituents and the beam (P_b) and target (P_t) polarization:

$$A_{||}^{meas}=\frac{1}{\mathrm{DF}P_bP_t}\frac{N^+/Q^+-N^-/Q^-}{N^+/Q^++N^-/Q^-}, \tag{4}$$

where $N^{+,-}$ are the counts and $Q^{+,-}$ are the integrated beam charges for positive and negative helicities.

We determined the dilution factor DF in Eq. (4) by approximating the contribution to the count rates from unpolarized target constituents (target foils, LHe coolant, and ^{15}N in ammonia) with the spectra taken on the carbon target. Some components of these two targets were the same (e.g., the LHe coolant and foils were present for the carbon target as well), and carbon, nitrogen, and even ^{4}He have similar binding energies per nucleon and Fermi momenta, suggesting that their inclusive electron scattering spectra are similar after correcting for the total number of target nucleons. (This assumption has since been verified to better than 3% with dedicated runs on a pure ^{15}N target during the second part of EG1.)

To account for the different number of nucleons in each target and different overall target thicknesses, we cross normalized the carbon target spectra to the ammonia target spectra. We determined a normalization constant A such that the two spectra had the same number of counts below a cutoff missing mass W_{cut}, well below the quasielastic peak. The cutoff ranged from $W_{cut}=0.835$ GeV at $Q^2=0.3$ (GeV/c)^2 to $W_{cut}=0.5$ GeV at $Q^2=1.2$ (GeV/c)^2, and was chosen so that the deuteron contribution was negligible, according to a Monte Carlo simulation of the deuteron wave function.

The dilution factor can then be written as

$$\mathrm{DF}=\frac{N_{ND_3}-AN_C}{N_{ND_3}}, \tag{5}$$

where the numerator is the count rate due to deuterium alone. The results of this method for an intermediate-Q^2 bin are shown in Fig. 3. The normalized carbon spectrum (circles) has been subtracted from the ammonia spectrum (solid triangles) to yield the deuteron spectrum (open triangles). The line indicates the result of our Monte Carlo simulation of the deuteron spectrum alone, which is based on quasielastic scattering (plane wave impulse approximation) and the Paris wave function [48] for the deuteron. The dilution factor for our experiment was around DF$\approx$0.2.

The second ingredient needed in Eq. (4) is the product of the beam and target polarizations. We measured both the beam polarization (with a Møller polarimeter) and the target polarization (using NMR) individually during the run. However, due to the small amount of target material and its inhomogeneous exposure to the electron beam, the NMR results were not very precise and reliable. Instead, we determined directly the product P_bP_t by extracting it from the measured asymmetry in the quasielastic region. For this purpose, we used inclusive quasielastic events $d(e,e')$ in the range 0.85 GeV$\leqslant W\leqslant$1.0 GeV.

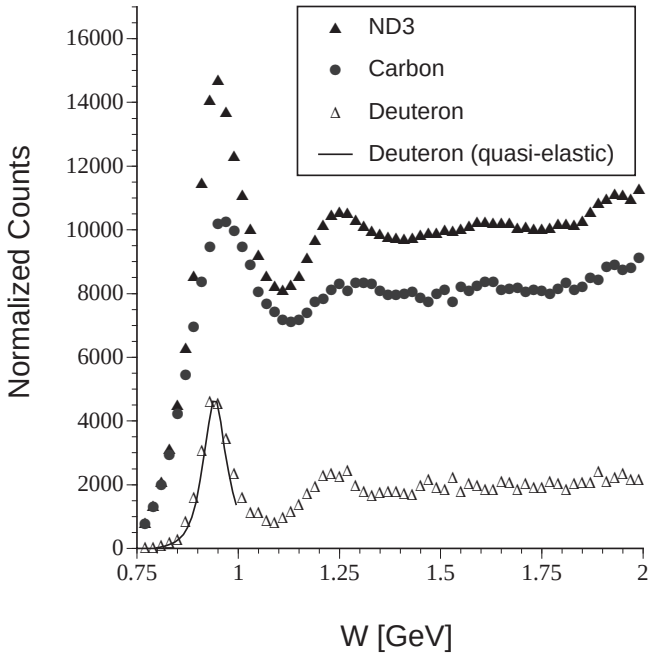

FIG. 3. Spectra of counts vs final state mass W from the polarized ND_3 target (solid triangles) and carbon target (circles) runs for the range $Q^2=0.5\pm0.1$ $(\mathrm{GeV}/c)^2$. The spectra have been cross normalized at low W. The deuteron spectrum (open triangles) is the difference between these two spectra. In the quasielastic peak region, it agrees well with a simulation using the Paris wave function for the deuteron (solid line).

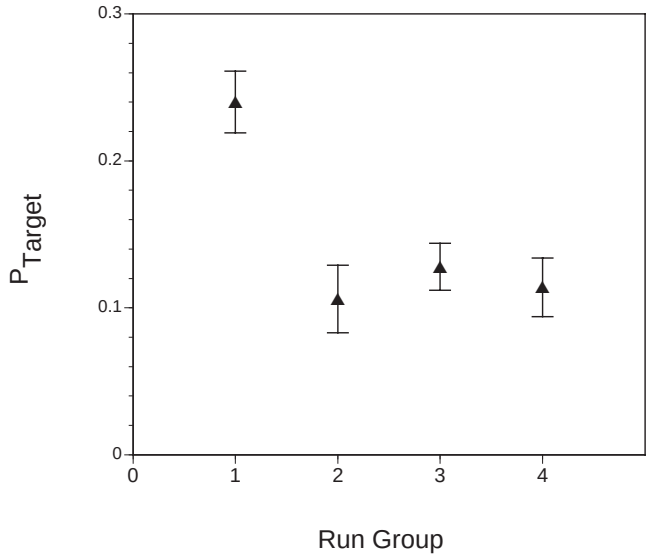

FIG. 4. Average target polarization for each of the four run groups determined by dividing the values of the product P_bP_t extracted from the quasielastic asymmetry by the beam polarization measured with a Møller polarimeter. The target polarization decreases over time due to beam exposure.

The asymmetry $A_{||}$ for elastic scattering from protons and neutrons can be calculated from known nucleon form factors with very little systematic uncertainty (less than 1–2 % in our kinematic region). We used our simulation of the deuteron wave function to calculate the expected asymmetry for inclusive quasielastic scattering within our kinematic cuts, which differed only slightly from the cross section-weighted average of the proton and neutron asymmetries. We used the dilution factor determined via the method described above to extract the product P_bP_t.

Due to the large kinematic coverage of CLAS, data on the quasielastic asymmetries were collected continuously and simultaneously with the inelastic asymmetry data. The extracted average polarization product P_bP_t for each of the four run groups is therefore a faithful representation of the running conditions for that group, with minimal systematic uncertainties. Our results are shown in Fig. 4, where we divided the product P_bP_t by the measured beam polarization to extract the target polarization. The results for each of the individual run groups have statistical errors on the order of 13%, which were included in the total statistical error of the asymmetries from each run group. The final results for the inelastic asymmetries are statistically weighted averages from the four run groups, with a contribution to their statistical errors from the polarization product of about 6.7% of their values.

D. Other backgrounds

After dividing out the dilution factor and the beam and target polarizations in Eq. (4), we corrected the extracted asymmetry for additional background contributions. These include contamination of the scattered electron sample by negative pions and pair-produced electrons, as well as contributions from polarized target constituents other than deuterium.

We already discussed the contribution from pions misidentified as electrons, which was less than 1% in all cases. A more important contribution comes from electrons that are decay products of neutral pions (either through the Dalitz decay $\pi^0\rightarrow\gamma e^+e^-$ or pair conversion of decay photons). The rate of electrons from these decays was estimated using the Wiser fit [49] for pion photoproduction and tested against the Monte Carlo code ''PYTHIA.'' We also measured directly the rate of positron production in each kinematic bin (again making use of the large acceptance of CLAS for both positively and negatively charged particles). This rate should be equal to that of electrons from charge-symmetric decays and was found to agree well with the Wiser fit. The asymmetry for positrons was found to be consistent with zero and in any case no larger than the asymmetry for electron scattering events. We used a parametrization of our results to estimate the fraction of detected electrons coming from these decays. This fraction was typically 1% for most of the kinematic region, but increased up to 20% at the highest W values. We corrected our data for this background by applying a further dilution factor to our asymmetries. Since we could not exclude a small nonzero asymmetry for these events, we assumed a systematic uncertainty equal to the size of this correction.

The nitrogen in our dynamically polarized ammonia target carries a small residual polarization, which leads to a partially polarized bound proton in ^{15}N. Possible additional polarized target species include isotopic impurities of ^{14}N and ^{1}H. Extensive experience with similar targets at SLAC [5]

shows that the corresponding corrections to the asymmetry are at most a few percent. We included the uncertainty due to these contributions in our systematic error.

Another potential contribution to the measured asymmetry comes from parity-violating electron scattering off all target constituents. However, at the low momentum transfers of our experiment, the expected asymmetry is less than 10^{-4} [50] and can be treated as another (small) systematic uncertainty.

E. Radiative corrections and models

The final step in the extraction of the desired ''Born asymmetry'' $A_{||}$ requires correcting the measured asymmetry for higher-order electromagnetic processes (internal radiative corrections) and electron energy loss through bremsstrahlung in the target before or after the scattering (external radiative corrections). These radiative corrections were applied separately to the numerator and the denominator of Eq. (3), which yields an additive (A_{RC}) and a multiplicative (F_{RC}) correction term:

$$A_{||}=A_{||}^{meas}/F_{RC}+A_{RC}. \tag{6}$$

Here, the factor $1/F_{RC}$ represents the increase of the denominator in Eq. (3) due to the radiative elastic and quasielastic tails that act like an additional dilution of the inelastic events. Correspondingly, the statistical error of the final result was scaled up by $1/F_{RC}$ as well.

Both components (F_{RC}, A_{RC}) were determined by running the code ''RCSLACPOL'' developed at SLAC [5]. This code uses parametrizations of all relevant input quantities (structure functions and form factors), as well as a model of our target, to calculate both fully radiated and Born cross sections and asymmetries. It is based on the approach developed by Kukhto and Shumeiko [51] for the internal corrections and by Tsai [52] for the external corrections, including the radiative depolarization of the beam due to external bremsstrahlung.

We used parametrizations of the world data on polarized and unpolarized structure functions and elastic form factors as input for the radiative correction code and to extract physics quantities of interest from the measured asymmetries. These parametrizations are described in Ref. [7] and are based on fits to unpolarized structure function data from NMC [53] and SLAC [54–57] and polarized structure function data from SLAC [40,4–8], CERN [1–3], and HERMES [9,10]. The nucleon form factors were taken from Ref. [58] with updated values for the ratio G_{Ep}/G_{Mp} from the recent Jefferson Lab experiment [59]. For the asymmetries A_1 and A_2 in the resonance region, we used parametrizations of resonance transition amplitudes from Ref. [30] (in the form of a computer code named ''AO'') and Ref. [60] (MAID) together with a fit of the SLAC data [41]. We also included our own preliminary asymmetry data in these fits. All fits were varied within reasonable errors or replaced with alternative existing fits to study the systematic dependence of our final results on these parametrizations.

F. Systematic errors

The total systematic error on our data ranges from 25% to 50% of the statistical error for the asymmetries and from 35% to 50% of the statistical error for the structure function g_1^d. The leading contributions to these systematic uncertainties come from radiative corrections (40–50 % of the total systematic error on average), uncertainties in the unpolarized structure functions needed to extract final physics results (also 40–50 % of the total), and the dilution factor (about 40%). We also considered the effect of finite resolution and errors in the measured kinematic variables (about 10% of the total). At higher Q^2 and especially higher W, pair-symmetric decay electrons also contributed significantly to the overall systematic uncertainty (15–20 % averaged over all kinematic bins and most of the systematic error at the kinematic limit). Finally, for the extraction of the spin structure function g_1^d and its integrals, some model assumption about the virtual photon asymmetry A_2 is needed (see Sec. IV) and leads to a further systematic error (up to 50%).

We accounted for each of these systematic errors by changing a relevant input parameter or model, and then repeating the entire analysis up to the final results, including the integrals of g_1^d over the measured region. We took the error as the deviation of the alternative results from the standard analysis. We added all uncorrelated systematic errors in quadrature. The final systematic errors are shown in the data tables in Sec. IV.

For the radiative correction errors, we varied all input models and parametrizations for the radiative code, including polarized and unpolarized structure functions, form factors, and the target model, within realistic limits. We also checked the accuracy of the peaking approximation by comparing the results with those from a full integration without approximations.

Similarly, we varied the models for the unpolarized structure functions F_1^d and $R=\sigma_L/\sigma_T$, which entered the extraction of g_1^d and the asymmetry $A_1^d+\eta A_2^d$ from our data (see Sec. IV). We used different fits of the world data [54,57,61] and studied their effect on the final physics results. In the case of the polarized structure function g_1^d and its integrals, we also varied the model for the asymmetry A_2^d from $A_2^d=0$ to the prediction by the MAID code and a simple parameterization based on the twist-2 result by Wandzura and Wilczek [62] that describes the SLAC data [8] well.

For the error introduced by the uncertainty in the dilution factor, we varied the cross normalization between the carbon and ammonia target data by an amount of 6%, consistent with the variations observed for different W and Q^2 ranges and possible differences in the ^{12}C and ^{15}N spectra. This yields an average variation of the dilution factor, Eq. (5), of 25%, making this error a safe upper bound for *all* systematic errors that are directly proportional to the measured asymmetry.

The CLAS momentum resolution and reconstruction effects were studied by moving all data points by 0.02 GeV in W and by recalculating the final results. The effect of this variation on the integrals of g_1^d also gave an upper limit to systematic errors due to the integration method, which con-

TABLE I. The measured virtual photon asymmetry $A_1^d+\eta A_2^d$ of the deuteron for $Q^2=0.27$–0.39 $(\mathrm{GeV}/c)^2$.

W (GeV)	$A_1^d+\eta A_2^d$	Stat. error	Syst. error
1.12	0.309	0.530	0.207
1.20	−0.273	0.208	0.061
1.28	−0.406	0.169	0.081
1.36	−0.223	0.191	0.069
1.44	−0.124	0.161	0.028
1.52	−0.077	0.131	0.017
1.60	−0.036	0.119	0.015
1.68	0.140	0.102	0.023
1.76	0.063	0.101	0.011
1.84	0.055	0.086	0.017
1.92	−0.254	0.080	0.028
2.00	−0.084	0.072	0.009

TABLE II. The measured virtual photon asymmetry $A_1^d+\eta A_2^d$ of the deuteron for $Q^2=0.39$–0.65 $(\mathrm{GeV}/c)^2$.

W (GeV)	$A_1^d+\eta A_2^d$	Stat. error	Syst. error
1.12	−0.327	0.267	0.191
1.20	−0.411	0.109	0.081
1.28	−0.316	0.090	0.061
1.36	−0.070	0.101	0.062
1.44	0.086	0.085	0.022
1.52	0.144	0.068	0.025
1.60	0.147	0.063	0.024
1.68	0.061	0.054	0.015
1.76	0.006	0.053	0.011
1.84	0.024	0.050	0.013
1.92	−0.045	0.047	0.013

sisted in a simple sum of all bins of size $\Delta W=0.02$ GeV, multiplied by the bin width in x.

Other systematic errors were either negligible or have already been described in the preceding section. We note that we do not have a significant *systematic* error from the beam and target polarization product, since they were directly determined from our data (with minimal theoretical uncertainty). In particular, the theoretical asymmetry $A_{||}^{elas}$ is only weakly dependent ($\pm 1\%$) on the elastic form factor ratio G_E/G_M for the proton. However, the *statistical* error of this method is not negligible and was included in the total statistical error of the final results.

IV. RESULTS

A. Virtual photon asymmetries

We extracted a combination of the virtual photon asymmetries, $A_1^d+\eta A_2^d$, from our data on $A_{||}$ using a parametrization [57] of the structure function R, via the relationship

$$A_{||}=D(A_1+\eta A_2), \tag{7}$$

where the virtual photon depolarization factor is given by $D=(1-\epsilon E'/E)/(1+\epsilon R)$ and $\eta=\epsilon\sqrt{Q^2}/(E-\epsilon E')$ (ϵ is the virtual photon polarization parameter, E is the beam energy, and E' is the scattered electron energy).

The extracted photon asymmetries $(A_1^d+\eta A_2^d)(W,Q^2)$ for three different Q^2 bins are listed in Tables I–III, together with their statistical and full systematic errors. We show the results for our intermediate Q^2 bin in Fig. 5, together with previous data from SLAC [5] and some model calculations. A comparison of the three different Q^2 bins can be found in Fig. 6.

Since we did not measure the asymmetry with the target polarization perpendicular to the electron beam ($A_\perp$), we cannot directly extract the asymmetry A_1^d or A_2^d. The interference term A_2 is limited by $|A_2|<\sqrt{R(A_1+1)/2}$, where the value of R is around 0.1–0.3 at $Q^2=0.5$ $(\mathrm{GeV}/c)^2$ [57] and the typical size of η for our experiment ranges from 0.1 at $W=2$ GeV to 1.2 right at the pion threshold ($W=1.08$ GeV). Correspondingly, the asymmetry A_2^d could contribute as much as 0.07 (high W) to 0.15 (at threshold) to the asymmetries shown in Figs. 5 and 6. However, according to our parametrization, this contribution should be more typically of order 0.02.

With this caveat, one can conclude that the data shown in Fig. 5 exhibit the expected behavior for asymmetry A_1^d. In the region of the $\Delta(1232)$ resonance, the asymmetry is strongly negative and fully compatible with the expectation $A_1^d=-0.5$ for the resonance contribution alone. Beyond $W=1.4$ GeV, the asymmetry becomes positive, indicating that helicity-$\frac{1}{2}$ transition amplitudes begin to dominate even at this rather low Q^2. However, even in the region of the S_{11} resonance the asymmetry is markedly smaller (around 0.15) than for the proton (around 0.5, see Ref. [5]), indicating that for the neutron alone the helicity-$\frac{3}{2}$ amplitude may still be larger. Figure 5 also shows the predicted full asymmetry from our parametrization and a prediction for the resonance contributions to A_1^d alone. The latter is based on the code AO [30], which uses a fit of exclusive pion electro and photoproduction data to parametrize resonant and Born pion production amplitudes. Apparently, the contribution from the resonances alone already describes the data well in the region of low to intermediate W, while nonresonant contributions (and maybe a sizable asymmetry A_2^d) are needed at high W. In

TABLE III. The measured virtual photon asymmetry $A_1^d+\eta A_2^d$ of the deuteron for $Q^2=0.65$–1.3 $(\mathrm{GeV}/c)^2$.

W (GeV)	$A_1^d+\eta A_2^d$	Stat. error	Syst. error
1.12	−0.529	0.223	0.125
1.20	−0.299	0.101	0.038
1.28	−0.106	0.083	0.025
1.36	−0.005	0.091	0.046
1.44	0.139	0.078	0.017
1.52	0.340	0.067	0.035
1.60	0.307	0.061	0.038
1.68	0.195	0.054	0.027
1.76	0.184	0.056	0.033

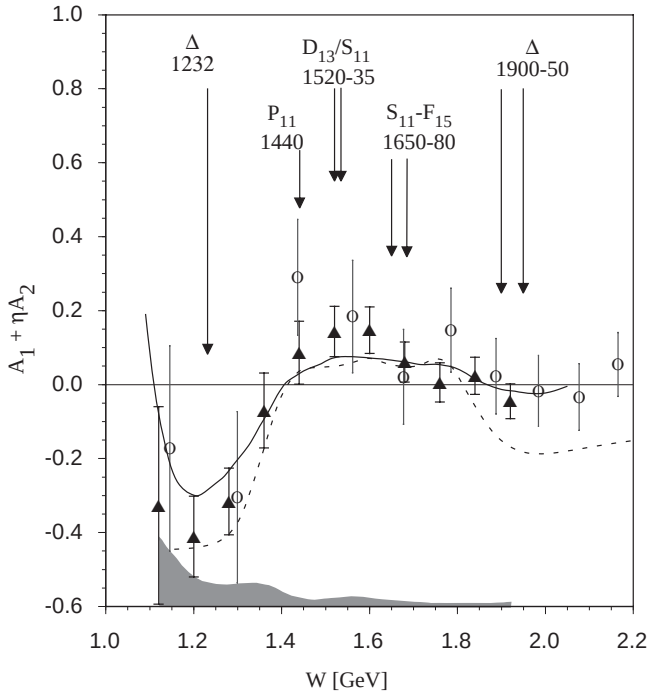

FIG. 5. $A_1^d+\eta A_2^d$ vs W for $Q^2=0.39$–0.65 $(\mathrm{GeV}/c)^2$. Our data points are shown as triangles with statistical errors only. The size of the systematic error is indicated by the shaded band at the bottom of the graph. Previous data from SLAC E143 [5] are shown as open circles with statistical and systematic errors combined. The positions of several prominent resonances are indicated by the labeled arrows. The solid line is our model parametrization of the world data (without nuclear corrections such as Fermi motion and off–shell effects) and the dashed line is the resonant contribution to A_1^d alone (from code AO).

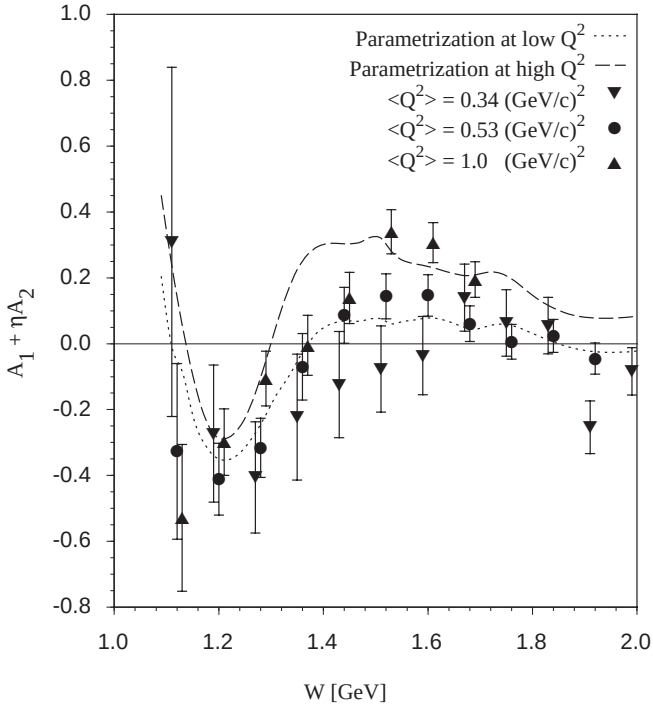

FIG. 6. Our data for three different bins in Q^2, together with statistical errors. (Systematic errors are highly correlated between different Q^2 bins and should have only minor effects on the observed Q^2 dependence). The long-dashed line shows our model parametrization of $A_1^d+\eta A_2^d$ for $Q^2=1.0$ $(\mathrm{GeV}/c)^2$ and the short-dashed line shows our model for $Q^2=0.34$ $(\mathrm{GeV}/c)^2$.

general, our data agree fairly well with model predictions and the existing SLAC data. However, they have significantly smaller statistical errors and better resolution in W, as well as coverage down to lower Q^2 than the SLAC data.

A comparison of our results for different Q^2 (see Fig. 6) shows a general trend toward more positive asymmetries for higher Q^2, especially in the region of the S_{11} and D_{11} resonances. This is in agreement with the expected transition from helicity-$\frac{3}{2}$ dominance at low Q^2 (and especially at the photon point, where it yields the negative value for the GDH sum rule), and helicity-$\frac{1}{2}$ dominance at higher Q^2. In the limit of very large Q^2, the asymmetry A_1^d in the resonance region should become close to 1, as predicted by pQCD as well as hyperfine-improved quark models and duality arguments. A similar behavior is observed for the proton asymmetries [5].

B. Spin structure function g_1^d

The spin structure function $g_1^d(W,Q^2)$ was calculated from the photon asymmetry $(A_1^d+\eta A_2^d)(W,Q^2)$ for each bin using

$$g_1^d(W,Q^2)=\frac{\tau}{1+\tau}\left(A_1^d+\frac{1}{\sqrt{\tau}}A_2^d\right)F_1^d(W,Q^2)$$
$$=\frac{\tau}{1+\tau}\left[(A_1^d+\eta A_2^d)+\left(\frac{1}{\sqrt{\tau}}-\eta\right)A_2^d\right]F_1^d(W,Q^2). \quad (8)$$

Here, $F_1^d\approx(F_1^p+F_1^n)/2$ represents the unpolarized structure function of the deuteron (per nucleon) and $\tau=\nu^2/Q^2$. Because of the partial cancellation of the two terms in $(1/\sqrt{\tau}-\eta)$, g_1^d is less sensitive to the asymmetry A_2. We list our results for g_1^d with their statistical and full systematic errors (including the uncertainty due to A_2) in Tables IV–VI.

In Fig. 7, we show our results for all three values of Q^2, plotted against the Nachtmann scaling variable $\xi=Q^2/M(\nu+q)$. This variable corresponds to Bjorken x at high Q^2 while it takes target nucleon mass corrections into account and therefore reduces "*kinematical* higher twist" scaling-violating effects at lower Q^2. Together with our data, we also show as reference the prediction for $g_1^d(\xi,Q^2=5\ (\mathrm{GeV}/c)^2)$ from our model. The assumption of local quark-hadron duality predicts that structure functions such as F_1 and g_1 should, on average, approach a universal scaling curve if plotted versus the variable ξ, even in the resonance region. This is confirmed down to rather low Q^2 in the case of the unpolarized structure function F_2^p [21,22]. Apparently,

TABLE IV. The spin structure function g_1^d of the deuteron for $Q^2=0.27-0.39$ (GeV/c)^2.

W (GeV)	g_1^d	Stat. error	Syst. error
1.12	0.033	0.058	0.042
1.20	−0.115	0.080	0.029
1.28	−0.172	0.074	0.033
1.36	−0.080	0.067	0.022
1.44	−0.059	0.067	0.015
1.52	−0.040	0.078	0.010
1.60	−0.022	0.073	0.013
1.68	0.112	0.074	0.020
1.76	0.058	0.075	0.011
1.84	0.048	0.065	0.015
1.92	−0.202	0.066	0.028
2.00	−0.070	0.066	0.012

local duality does not work as well for the *polarized* structure function g_1^d at high values of ξ where the asymmetry is dominated by the Δ resonance and therefore is negative. Overall, the approach to the ''asymptotic value'' for $Q^2=5$ (GeV/c)^2 seems to be relatively slow; only our highest Q^2 bin shows fairly good agreement beyond the region of the Δ resonance.

C. Integrals

We calculated the integrals $\Gamma_1^d(Q^2)=\int g_1^d(x,Q^2)dx$ for our results on $g_1^d(x,Q^2)$ over the (ordinary) Bjorken variable x for four different Q^2 bins, beginning at quasifree pion production threshold ($W=1.08$ GeV) up to the kinematic limit of our data. [The first two Q^2 bins are the same as shown in Tables IV and V, while we split the last bin into two halves, from $Q^2=0.65$ to 0.92 (GeV/c)^2 and from $Q^2=0.92$ to 1.3 (GeV/c)^2.] We expect that these integrals are close to an incoherent average over the individual nucleons (proton and neutron) in deuterium, reduced by the D-state correction factor $(1-1.5P_D)$, where $P_D\approx 0.05$ is the deuteron D-state probability. The results are shown in the third column of Table VII and the upper kinematic limits for W are listed in

TABLE V. The spin structure function g_1^d of the deuteron for $Q^2=0.39-0.65$ (GeV/c)^2.

W (GeV)	g_1^d	Stat. error	Syst. error
1.12	−0.025	0.018	0.004
1.20	−0.088	0.025	0.017
1.28	−0.083	0.024	0.011
1.36	−0.008	0.023	0.014
1.44	0.024	0.024	0.007
1.52	0.075	0.029	0.012
1.60	0.080	0.028	0.014
1.68	0.046	0.030	0.012
1.76	0.016	0.031	0.011
1.84	0.028	0.030	0.013
1.92	−0.016	0.031	0.013

TABLE VI. The spin structure function g_1^d of the deuteron for $Q^2=0.65-1.3$ (GeV/c)^2.

W (GeV)	g_1^d	Stat. error	Syst. error
1.12	−0.022	0.008	0.004
1.20	−0.029	0.011	0.003
1.28	−0.010	0.011	0.004
1.36	0.003	0.011	0.007
1.44	0.024	0.013	0.005
1.52	0.086	0.016	0.011
1.60	0.089	0.016	0.013
1.68	0.072	0.018	0.013
1.76	0.082	0.021	0.017

the second column. These upper W bounds correspond to lower limits of $x=(0.1,0.15,0.21,0.32)$ for the four Q^2 bins, respectively.

We use our model to estimate the contribution to the integral below these limits and show the resulting ''full'' integrals and their systematic errors in the last two columns of Table VII. These systematic errors include a contribution from the uncertainty of this extrapolation to $x=0$. To estimate this uncertainty, we studied the variation of the low-x contribution according to different fits to the world data; also, since there are few high-precision data below $x=0.03$, we added a systematic error equal to the value of the

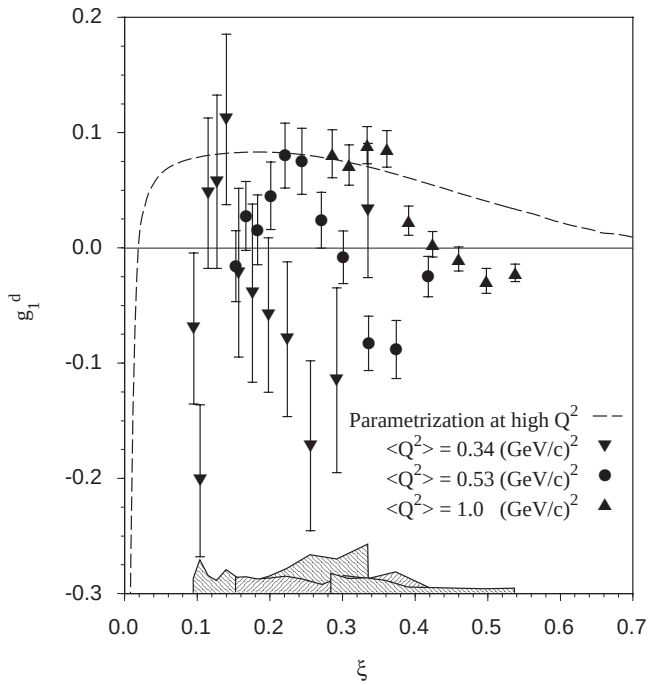

FIG. 7. The spin structure function g_1^d for the deuteron at three different values of Q^2, plotted against the Nachtmann variable ξ together with an extrapolation of a fit to the deep inelastic data at $Q^2=5$ (GeV/c)^2. Following standard conventions, all values are normalized to the number of nucleons in deuterium. The error bars are statistical only, while the shaded bands indicate systematic error bars for the three datasets.

TABLE VII. The first moments of the spin structure function g_1^d of the deuteron. Following standard convention, the integral is normalized to the number of nucleons in deuterium. Q^2 is in $(\mathrm{GeV}/c)^2$ and W_{max} in GeV.

Q^2	$W_{\max}$	Meas. Γ_1	Stat. error	Syst. error	Full Γ_1	Syst. error
0.34	2.00	−0.027	0.012	0.005	−0.034	0.008
0.53	2.00	−0.008	0.004	0.002	−0.013	0.007
0.79	1.96	0.008	0.003	0.003	0.009	0.008
1.10	1.80	0.007	0.003	0.002	0.016	0.009

integral from $x=0$ up to 0.03. Due to the large theoretical uncertainty about the shape of the spin structure functions at very low x and the absence of high-precision data in this region, the error on this extrapolation may be even larger than that indicated by our systematic error estimate (see below).

Our results for the first moment $\Gamma_1^d(Q^2)$ of the spin structure function g_1^d are shown in Fig. 8. The solid line at higher Q^2 is a fit to the world's data in the DIS region including QCD corrections up to second power in the strong coupling constant. The dotted line indicates the slope for the integral at $Q^2=0$ predicted by the GDH sum rule (we use the incoherent sum of the results for the proton and for the neutron, normalized to two). The short-dashed line is the result from the code AO [30] for the contribution from the nucleon resonances only. The long-dashed line by Burkert and Ioffe [31,32] is the AO result plus a term that depends smoothly on Q^2 and interpolates between the part that is missing at $Q^2=0$ to saturate the GDH sum rule and the full value of Γ_1 in the high-Q^2 limit. Figure 8 also shows the prediction from the model by Soffer and Teryaev [28,29] (dot-dashed line). They use an interpolation of the integral over the structure function $g_T=g_1+g_2$, which converges to Γ_1 at high Q^2 and remains positive down to the photon point where its slope is given by a combination of the nucleon charge and anomalous magnetic moment. They subtract the contribution from the integral over g_2 (which is related to nucleon form factors via the Burkardt-Cottingham sum rule) to obtain the integral Γ_1 alone. The same authors have recently published a new parametrization of the proton-neutron difference integral for all Q^2 [63] which might change the curve for the deuteron shown here. The solid triangles are based on EG1 data alone and the open triangles include the estimated contribution to the integral from beyond our kinematic limits. The inner error bars are statistical and the outer error bars represent the systematic errors added in quadrature. They include the uncertainty on the estimated low-x contribution for the full integrals (open triangles).

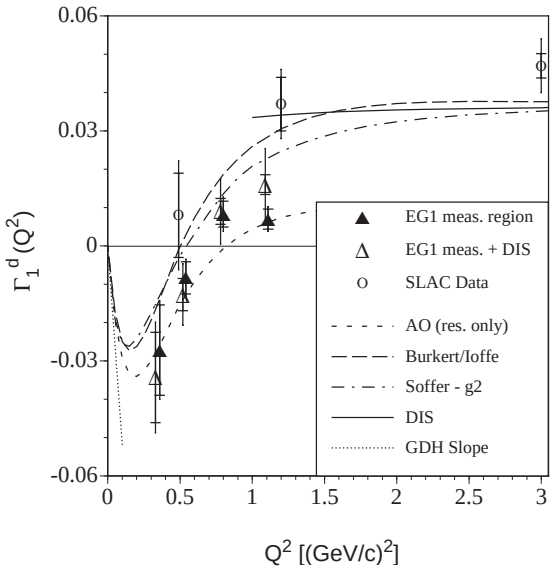

FIG. 8. The first moment of the spin structure function g_1^d of the deuteron (per nucleon). See explanations in text.

The first conclusion one can draw from Fig. 8 is that the integral over our measured region (essentially the resonance region) is in rather good agreement with the prediction of the AO parametrization for resonance contributions only. The data follow the predicted trend from negative values at small Q^2, where the Δ resonance contributes most of the integral and most other resonances are also dominated by the helicity-$\frac{3}{2}$ transition amplitude, to positive values at higher Q^2, where the helicity-$\frac{1}{2}$ amplitude begins to take over and the importance of the Δ is diminished. Since we did not include Born terms or other nonresonant terms in the curve labeled AO, one can conclude that these terms must contribute relatively little to the integral over the resonance region in the case of the deuteron. This may be due to a partial cancellation between the asymmetry of the proton (which is likely positive for these terms) and that of the neutron.

Extrapolating the integral down to $x=0$ seems to change the results only moderately (in the negative direction at low Q^2 and towards more positive values at higher Q^2). This can be understood again as a cancellation between a strongly negative-going trend of the structure function $g_1^n(x)$ as x goes to zero and a more positive trend for $g_1^p(x)$, according to existing DIS data and next-to-leading order (NLO) perturbative analyses [14,64]. However, at present, our understanding of the behavior of spin structure functions at very low x is still incomplete, making this extrapolation rather uncertain (as it is in the DIS region). Therefore, the error bars on our open triangles may still underestimate that uncertainty. The emergence of new information on the low-x behavior of spin structure functions over the past five years is responsible for most of the apparent disagreement between our quoted results and those from the E143 experiment at SLAC. The integrals over the resonance region alone agree fairly well with the SLAC data (to within 1.1 standard deviations); how-

ever, the extrapolation beyond $W=2$ GeV is much more negative for the parametrization used in the present analysis and would move the SLAC data points down by about 0.008 and 0.015 at $Q^2=0.5$ and 1.1 $(\mathrm{GeV}/c)^2$, respectively. With this proviso, our data are (marginally) consistent with the SLAC data, but have much improved statistical errors and cover lower Q^2.

Our data lie somewhat below both phenomenological predictions for the full integral shown in Fig. 8, suggesting a slower transition from the negative values near the photon point to the positive asymptotic value at high Q^2. The zero crossing appears to occur somewhere between $Q^2=0.5$ $(\mathrm{GeV}/c)^2$ and $Q^2=0.8$ $(\mathrm{GeV}/c)^2$, significantly later than in the case of the proton [5]. However, the systematic errors are highly correlated point-to-point so that the deviation from the predictions by Burkert and Ioffe [31,32] and by Soffer and Teryaev [28,29] is not highly significant.

V. SUMMARY AND OUTLOOK

In this paper, we report first results on deuterium for inclusive spin structure functions in the nucleon resonance region from the EG1 program at Jefferson Lab. These data significantly expand the kinematic coverage and statistical precision beyond the only previous data from SLAC [41]. We find generally reasonable agreement between these two datasets and various model predictions and parametrizations. In particular, the importance and the negative asymmetry of the Δ resonance is confirmed, as is the general trend to more positive asymmetries at higher Q^2 and W.

The spin structure function g_1^d is less positive than for the proton case [5], indicating that the neutron contribution is mostly negative in our kinematic region. While $g_1^d(\xi,Q^2)$ seems to be approaching the DIS scaling curve for large W and Q^2, there are significant deviations from ''local duality,'' again mostly due to the Δ resonance.

The integral over g_1^d follows the expected trend in general, rising towards the DIS limit at the highest measured Q^2 while dropping rapidly below zero towards our lowest Q^2 point. Clearly, neither the kinematic reach (in W and Q^2) nor the statistical precision of the present dataset allow a definite statement about the validity of (or the approach towards) the GDH sum rule limit. However, our data constrain the general trend required of any theory that aims to describe the spin structure of the nucleon over the full range of length scales, from the real photon point to the scaling limit.

Spin structure function data on the deuteron, together with the corresponding proton results, should, in principle, allow us to separate the different isospin contributions to the resonant and nonresonant asymmetries. However, the first run of EG1 analyzed here did not yield enough statistical precision to make a direct separation of proton and neutron contributions to the deuteron asymmetry feasible. However, we plan to submit results on the integral Γ_1 for the neutron and the proton-neutron difference, extracted from our data on the proton and the deuteron, in a separate paper. In the meantime, the complete EG1 dataset has been collected in a second run, which will yield a nearly tenfold improvement in statistics for the deuteron and a wider coverage towards both lower and higher Q^2 and higher W. Once analyzed, this vastly larger data set will allow us to investigate in detail resonance electroproduction on the neutron and the approach of the first moment of g_1^d and g_1^n towards the GDH sum rule at the real photon point.

ACKNOWLEDGMENTS

We would like to acknowledge the outstanding effort of the Accelerator, Target Group, and Physics Division staff at TJNAF that made this experiment possible. This work was supported by the U.S. Department of Energy, the Italian Istituto Nazionale di Fisica Nucleare, the U.S. National Science Foundation, the French Commissariat à l'Energie Atomique, the French Centre National de la Recherche Scientifique, and the Korea Science and Engineering Foundation. The Southeastern Universities Research Association (SURA) operates the Thomas Jefferson National Accelerator Facility for the U.S. Department of Energy under Contract No. DE-AC05-84ER40150.

[1] J. Ashman *et al.*, EMC Collaboration, Nucl. Phys. **B328**, 1 (1989).
[2] D. Adams *et al.*, SMC Collaboration, Phys. Rev. D **56**, 5330 (1997).
[3] D. Adams *et al.*, SMC Collaboration, Phys. Lett. B **396**, 338 (1997).
[4] P.L. Anthony *et al.*, E142 Collaboration, Phys. Rev. D **54**, 6620 (1996).
[5] K. Abe *et al.*, E143 Collaboration, Phys. Rev. D **58**, 112003 (1998).
[6] K. Abe *et al.*, E154 Collaboration, Phys. Rev. Lett. **79**, 26 (1997).
[7] P.L. Anthony *et al.*, E155 Collaboration, Phys. Lett. B **493**, 19 (2000).
[8] P. L. Anthony *et al.*, E155 Collaboration, Phys. Lett. B **553**, 18 (2003).
[9] K. Ackerstaff *et al.*, HERMES Collaboration, Phys. Lett. B **404**, 383 (1997).
[10] A. Airapetian *et al.*, HERMES Collaboration, Phys. Lett. B **442**, 484 (1998).
[11] M. Stratmann and W. Vogelsang, Phys. Rev. D **64**, 114007 (2001).
[12] M. Gluck, E. Reya, M. Stratmann, and W. Vogelsang, Phys. Rev. D **63**, 094005 (2001).
[13] D. de Florian and R. Sassot, Phys. Rev. D **62**, 094025 (2000).
[14] K. Abe *et al.*, E154 Collaboration, Phys. Lett. B **405**, 180 (1997).
[15] J.D. Bjorken, Phys. Rev. **148**, 1467 (1966).
[16] J.D. Bjorken, Phys. Rev. D **1**, 1376 (1970).
[17] E. Stein, P. Gornicki, L. Mankiewicz, and A. Schafer, Phys. Lett. B **353**, 107 (1995).

[18] E. Stein, P. Gornicki, L. Mankiewicz, A. Schafer, and W. Greiner, Phys. Lett. B **343**, 369 (1995).
[19] I.I. Balitsky, V.M. Braun, and A.V. Kolesnichenko, Phys. Lett. B **242**, 245 (1990).
[20] E.D. Bloom and F.J. Gilman, Phys. Rev. Lett. **25**, 1140 (1970).
[21] I. Niculescu *et al.*, Phys. Rev. Lett. **85**, 1186 (2000).
[22] I. Niculescu *et al.*, Phys. Rev. Lett. **85**, 1182 (2000).
[23] C.E. Carlson and N.C. Mukhopadhyay, Phys. Rev. D **58**, 094029 (1998).
[24] S. Simula, M. Osipenko, G. Ricco, and M. Taiuti, Phys. Rev. D **65**, 034017 (2002).
[25] S.B. Gerasimov, Yad. Fiz. **2**, 598 (1966) [Sov. J. Nucl. Phys. **2**, 430 (1966)].
[26] S.D. Drell and A.C. Hearn, Phys. Rev. Lett. **16**, 908 (1966).
[27] M. Anselmino, B.L. Ioffe, and E. Leader, Yad. Fiz. **49**, 214 (1989) [Sov. J. Nucl. Phys. **49**, 136 (1989)].
[28] J. Soffer and O.V. Teryaev, Phys. Rev. D **51**, 25 (1995).
[29] J. Soffer and O.V. Teryaev, Phys. Rev. D **56**, 7458 (1997).
[30] V. Burkert and Z.-j. Li, Phys. Rev. D **47**, 46 (1993).
[31] V.D. Burkert and B.L. Ioffe, Phys. Lett. B **296**, 223 (1992).
[32] V.D. Burkert and B.L. Ioffe, Zh. Eksp. Teor. Fiz. **105**, 1153 (1994) [JETP **78**, 619 (1994)].
[33] X.-D. Ji and P. Unrau, Phys. Lett. B **333**, 228 (1994).
[34] H. Burkhardt and W.N. Cottingham, Ann. Phys. **56**, 453 (1970).
[35] L.P. Kaptari, A.Y. Umnikov, C. Ciofi degli Atti, S. Scopetta, and K.Y. Kazakov, Phys. Rev. C **51**, 52 (1995).
[36] G. Piller, W. Melnitchouk, and A.W. Thomas, Phys. Rev. C **54**, 894 (1996).
[37] C. Ciofi degli Atti, L.P. Kaptari, S. Scopetta, and A.Y. Umnikov, Phys. Lett. B **376**, 309 (1996).
[38] C. Ciofi degli Atti, S. Scopetta, A.Y. Umnikov, and L.P. Kaptari, nucl-th/9602026.
[39] H. Arenhovel, G. Kress, R. Schmidt, and P. Wilhelm, Nucl. Phys. **A631**, 612c (1998).
[40] G. Baum *et al.*, Phys. Rev. Lett. **45**, 2000 (1980).
[41] K. Abe *et al.*, E143 Collaboration, Phys. Rev. Lett. **78**, 815 (1997).
[42] R. De Vita *et al.*, CLAS Collaboration, Phys. Rev. Lett. **88**, 082001 (2002).
[43] M. Amarian *et al.*, Jefferson Lab E94010 Collaboration, Phys. Rev. Lett. **89**, 242301 (2002).
[44] B. Mecking *et al.*, Nucl. Instrum. Methods (to be published).
[45] C. Keith *et al.*, Nucl. Instrum. Methods (to be published).
[46] A. Abragam and M. Goldman, Rep. Prog. Phys. **41**, 396 (1978).
[47] D. Crabb and W. Meyer, Annu. Rev. Nucl. Part. Sci. **47**, 67 (1997).
[48] M. Lacombe *et al.*, Phys. Rev. C **21**, 861 (1980).
[49] D. Wiser, Ph.D. thesis, University of Wisconsin, 1977.
[50] C.Y. Prescott *et al.*, Phys. Lett. **84B**, 524 (1979).
[51] T.V. Kukhto and N.M. Shumeiko, Nucl. Phys. **B219**, 412 (1983).
[52] Y.-S. Tsai, Rev. Mod. Phys. **46**, 815 (1974).
[53] M. Arneodo *et al.*, NMC Collaboration, Phys. Lett. B **364**, 107 (1995).
[54] A. Bodek *et al.*, Phys. Rev. D **20**, 1471 (1979).
[55] L.H. Tao *et al.*, E140X Collaboration, Z. Phys. C **70**, 387 (1996).
[56] L.M. Stuart *et al.*, Phys. Rev. D **58**, 032003 (1998).
[57] K. Abe *et al.*, E143 Collaboration, Phys. Lett. B **452**, 194 (1999).
[58] P. Bosted, Phys. Rev. C **51**, 409 (1995).
[59] M.K. Jones *et al.*, Jefferson Lab Hall A Collaboration, Phys. Rev. Lett. **84**, 1398 (2000).
[60] D. Drechsel *et al.*, Nucl. Phys. **A645**, 145 (1999).
[61] G. Ricco, S. Simula, and M. Battaglieri, Nucl. Phys. **B555**, 306 (1999).
[62] S. Wandzura and F. Wilczek, Phys. Lett. **72B**, 195 (1977).
[63] J. Soffer and O.V. Teryaev, Phys. Lett. B **545**, 323 (2002).
[64] P.L. Anthony *et al.*, E155 Collaboration, Phys. Lett. B **463**, 339 (1999).